fractal and fractional

MDPI

Article

Minkowski–Sierpinski Fractal Structure-Inspired 2 × 2 Antenna Array for Use in Next-Generation Wireless Systems

Arshad Karimbu Vallappil [1,*], Bilal A. Khawaja [1,*], Mohamad Kamal A. Rahim [2], Muhammad Uzair [1], Mohsin Jamil [3] and Qasim Awais [4]

[1] Department of Electrical Engineering, Faculty of Engineering, Islamic University of Madinah, P.O. Box 170, Madinah 41411, Saudi Arabia
[2] Advance RF and Microwave Research Group (ARFMRG), School of Electrical Engineering, Faculty of Engineering, Universiti Teknologi Malaysia, UTM Johor Bahru, Johor Bahru 81310, Johor, Malaysia
[3] Department of Electrical and Computer Engineering, Faculty of Engineering and Applied Science, Memorial University of Newfoundland, St. John's, NL A1C 5S7, Canada
[4] Department of Electronics Engineering, Fatima Jinnah Women University Rawalpindi, Old Presidency, Rawalpindi 46000, Pakistan
* Correspondence: arshadkv@iu.edu.sa (A.K.V.); 7166@iu.edu.sa (B.A.K.)

Abstract: In this paper, the design, simulation, fabrication, and characterization study of a low-cost and directional hybrid four-element (2 × 2 configuration) Minkowski–Sierpinski fractal antenna array (MSFAA) for the high-efficiency IEEE 802.11ax WLANs (Wi-Fi 6E) and the sub-6 GHz 5G wireless system is presented. Each element of the array is separated by 0.7 λ_0. The complete four-element fractal antenna array system includes designing the single-element Minkowski–Sierpinski fractal antenna using two different substrates for performance comparison and an equal-split Wilkinson power divider (WPD) to achieve power division and to form a feed network. The single-element antenna, four-element fractal antenna array, and WPDs are fabricated using a flame-resistant (FR4) glass epoxy substrate with a dielectric constant (ε_r) of 4.3 and thickness (h) of 1.66 mm. For performance comparison, a high-end Rogers thermoset microwave material (TMM4) substrate is also used, having ε_r = 4.5 and h = 1.524mm, respectively. The designed four-element fractal antenna array operates at the dual-band frequencies of 4.17 and 5.97 GHz, respectively. The various performance parameters of the antenna array, such as return loss, bandwidth, gain, and 2D and 3D radiation patterns, are analyzed using CST Microwave Studio. The fabricated four-element antenna array provides the bandwidth and gain characteristic of 85 MHz/4.19 dB and 182 MHz/9.61 dB at 4.17 and 5.97 GHz frequency bands, respectively. The proposed antenna array design gives an improvement in the bandwidth, gain, and radiation pattern in the boresight at both frequencies. In the IEEE 802.11 ax WLANs (Wi-Fi 6E) deployments and the upcoming 5G wireless and satellite communication systems, it is critical to have directional antenna arrays to focus the radiated power in any specific direction. Therefore, it is believed that the proposed dual-band four-element fractal antenna array with directional radiation patterns can be an ideal candidate for the high-efficiency IEEE 802.11ax WLANs (Wi-Fi 6E) and the upcoming 5G wireless and satellite communication systems.

Keywords: fifth-generation (5G); antenna array; Minkowski; Sierpinski; fractal antenna; Wilkinson power divider (WPD); IEEE 802.11ax; Wi-Fi 6E

Citation: Vallappil, A.K.; Khawaja, B.A.; Rahim, M.K.A.; Uzair, M.; Jamil, M.; Awais, Q. Minkowski–Sierpinski Fractal Structure-Inspired 2 × 2 Antenna Array for Use in Next-Generation Wireless Systems. *Fractal Fract.* **2023**, *7*, 158. https://doi.org/10.3390/fractalfract7020158

Academic Editor: Peter Z. Petkov

Received: 1 November 2022
Revised: 26 January 2023
Accepted: 1 February 2023
Published: 5 February 2023

1. Introduction

Over the last two decades, there has been an exponential growth in wireless communication systems with enhanced data-rate requirements of the end-users due to the availability of new and smart wireless devices [1,2]. Moreover, the upsurge of bandwidth-hungry applications such as live video streaming, peer-to-peer (P2P), and virtual/augmented reality (VR/AR) online gaming, and the ever-increasing urge of the end-users to stay online all the time has fueled this manifold growth [2,3]. The number of wireless users is radically

increasing, and currently, ~23 billion wireless devices are connected to the internet. It is predicted that these devices will increase to 75 billion by 2025 [4]. Initially, in order to meet the ever-increasing high throughput per user demand both for home users and in high-density places such as offices, stadiums, train stations, and airports, etc., the IEEE introduced an enhanced version of IEEE 802.11ac [5] standard, which is commonly referred to as IEEE 802.11ax or Wi-Fi6 [6]. The 802.11ax has the ability to deliver 9.6 GB/s data rates, which is 37% higher than its predecessor, 802.11ac [6]. Another important feature of this technology is that it exploits both the 2.4 and 5 GHz frequency bands simultaneously. In the future, 802.11ax technology will also be available in the 6 GHz band as part of Wi-Fi 6E [6]. Then, technological growth of the fifth-generation (5G) wireless systems [2,3] will be needed to meet this high demand for the network. The emerging 5G system will provide the end-users with benefits such as improved data rates, less power dissipation, and reduced over-the-air latency, with an improved overall system capacity of several billion users [1–3]. Another important feature of the 5G technology is the exploitation of both microwave (around 3–6 GHz) and millimeter-wave (mmW) frequency bands [1–3,7]. This provides enhanced spectral utilization and leads to the requirement of antenna arrays with beam-steering capabilities to focus radiated power in any specific direction. The 5G technology is expected to provide enhanced quality of service (QoS) with constant connectivity to end-users who demand anytime, anywhere, and with-anything connectivity [2–7].

The primary driver in the development of high throughput wireless local area networks (WLANs) such as 802.11ax (Wi-Fi 6E), as well as 5G wireless systems, is the requirement of compact structure antennas that provide wide bandwidth for mobile and other wireless devices. In modern WLANs, planar microstrip patch antennas (MPAs) are preferred because of their compactness, flexible structure, low profile and cost, simplicity of design, and ability to conform with printed circuit boards (PCBs) [8,9]. A conventional MPA resonates at a single frequency band and offers low gain and narrow bandwidth, although by the insertion of different stubs and slots to change the current path, the MPA can be made to cover multiple frequency bands [9,10]. Using the MPA design techniques, many researchers [5,10–14] have proposed different antenna array designs for 5G wireless systems operating at both microwave and mmW frequency bands.

Recently, there has been much interest in fractal antenna design techniques for the upcoming 5G system [14–17]. Fractal antenna structures are preferred because they not only help with the physical antenna size reduction, but also aid in the designing of miniaturized multiband antennas at a low cost. Mandelbrot et al. [18] proposed the first fractal geometry. Since then, many different fractal antenna structures have been proposed in the literature, which include the Sierpinski gasket, Minkowski and Sierpinski carpet, Cantor set, and Koch curves geometries, etc. [14–17,19–32]. The issue with a conventional dual-band fractal array antenna is that it offers limited bandwidth and low gain due to the constraint of mutual coupling. In [23], it is shown that the circular fractal antenna array with a partial ground plane generates multiple frequency bands with a maximum bandwidth of ~500 MHz and a gain of 5.94 dB, respectively. In [24], a miniaturized and compact two-fractal antennas with Koch-fed obtrusion/slot with the asymmetric ground plane (AGP) is presented, which shows an improved bandwidth of 100 MHz and a gain of 5 dB. In [25], an eight-element linear array of fractal antennas based on the Koch snowflake design technique is presented; the array develops a 15.18 dB gain with 105 MHz bandwidth and a radiation efficiency of 72.12%. In [26], the researchers presented a Sierpinski fractal antenna array with a coplanar waveguide (CPW) feed, which leads to multiband behavior. This antenna array design gives a bandwidth of 90 MHz and a gain of 11 dB. A complementary Sierpinski gasket fractal antenna array for portable multiple-input multiple-output (MIMO) wireless devices is presented in [28], which gives a single frequency band that shows a gain of 10 dB with a bandwidth of 400 MHz. Article [29] presents a four-branch array antenna system comprising sixteen rectangular and circular patch elements. The presented antenna operates at dual-band, which is at 2.54 and 5.64 GHz. The dual-band antenna array is appropriate for Wi-Fi, WiMAX, Bluetooth, Zigbee, and ISM applications. It keeps return

loss at −10 dB while having better gain and directivity across both operating bands. In article [30], a dual-band array antenna system with high gain and a compact design is presented. It can be used in 5G communication systems. There are two monopole elements in the antenna array. The isolation between these two monopole elements was substantially increased, and the dimension of the antenna array was lowered by protruding the ground branches in the metal plane. A tri-band fractal hexagonal antenna array for 5G mobile networks is presented in [31]. Return loss improved with this design, and it also produces better radiation characteristics. As per the literature review presented here, most of the discussed designs demonstrate either improvement in gain or bandwidth, and most of the presented radiation patterns in the literature are omnidirectional in nature. For the design presented in this paper, we have concentrated on dual-band frequency behavior with the improvement in bandwidth, gain, efficiency, and radiation pattern in the boresight at the same time, respectively.

Therefore, this paper initially presents a single-element dual-band operation Minkowski–Sierpinski fractal antenna design using two different substrates, i.e., a high-end Rogers TMM4 substrate and a low-end FR4 substrate. The performance of both antenna designs is compared. Then, a hybrid four-element (2 × 2 configuration) dual-band Minkowski–Sierpinski fractal antenna array (MSFAA) design is proposed for 802.11ax (Wi-Fi 6E), sub-6 GHz 5G, and next-generation wireless applications. The proposed single-element antenna and the 2 × 2 configuration antenna array are operating at 4.17 and 5.97 GHz frequency bands, respectively. The proposed fractal antenna array has many attractive features, such as a high gain and directional radiation pattern at the boresight. Both features make the proposed antenna array a promising candidate for the 802.11ax (Wi-Fi 6E), sub-6 GHz 5G, Internet of Things (IoT), and next-generation wireless applications. All four elements of the 2 × 2 configuration fractal antenna array are individually mounted on an aluminum sheet, which acts as a holding mount and extended ground plane for the individual array elements. Then, a delta-stub-based 1 × 2 Wilkinson power divider (WPD) feed network is also designed, which is used with the help of coaxial cables to feed the individual array elements. The rest of the paper is organized as follows: Section 2 briefly discusses the WPD design configuration as well as its simulation and measured results. The single-element fractal antenna design and its results, as well as the four-element fractal antenna array design and characterization results, including return loss (S_{11}), 2D and 3D radiation patterns, gain, and surface current distribution, are discussed and summarized in Section 3. Section 4 provides a comparison of the results and overall discussion of the paper and its findings, and finally, Section 5 draws conclusions.

2. Delta-Stub-Based Wilkinson Power Divider (WPD) Design Configuration and Characterization Results

The WPD [8] is characterized as a three-port lossless network, which provides isolation between the output ports when they are matched; only the reflected power is typically dissipated. The power to the input port-1 can be split into two ports with the same amplitude. In order to realize a two-way equal-split in signal power, quarter-wave ($\lambda/4$ impedance) transformers with a characteristic impedance of Z_o are used. The equivalent circuit of the conventional WPD is shown in Figure 1a. The simulated design of the proposed WPD using CST Microwave Studio is shown in Figure 1b, whereas the fabricated prototype is shown in Figure 1c. FR4 glass epoxy substrate (ε_r = 4.3 and h = 1.66 mm) is selected for this purpose.

The three ports of the WPD are labeled as port-1, port-2, and port-3, respectively, as shown in Figure 1a–c. The straight quarter-lambda split Section 1 × 2 WPD is the conventional design, which is initially presented in Figure 1a. In the WPD, the power at the output ports, port-2 and port-3, is half the power of the input from port-1. Therefore, the insertion loss at each of the output ports is −3 dB. The width of the 50 Ω transmission line is taken as 3 mm, whereas the length and width of the quarter-wave transformers with an impedance of 70.71 Ω are taken as 7 mm × 1.5 mm. The fabricated prototype of

the WPD has overall dimensions of 20 × 36 mm, as shown in Figure 1c. Two delta-stubs with a length × width of 2.38 × 0.74 mm are introduced on both sides of the quarter-wave transformers for improved impedance matching and wide bandwidth characteristics of the WPD.

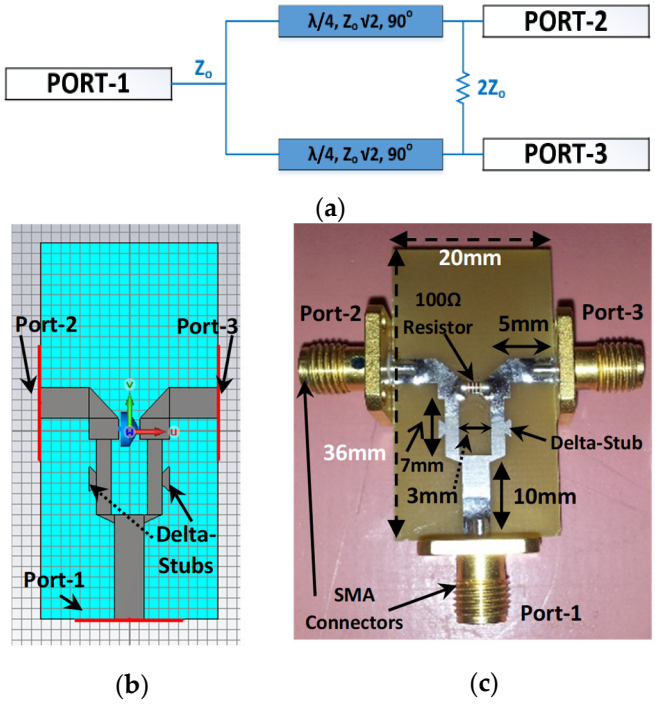

Figure 1. Shows (**a**) transmission-line circuit of an equal-split WPD [8], (**b**) simulated design, and (**c**) fabricated prototype of delta-stub-based 1 × 2 WPD.

Figure 2a,b shows the simulated and measured S-parameter response of the delta-stub-based 1 × 2 WPD at the bandwidth of 3.5–6.5 GHz. It can be observed from the results in Figure 2b that there is almost equal power division between the two output ports, port-2 and port-3, respectively.

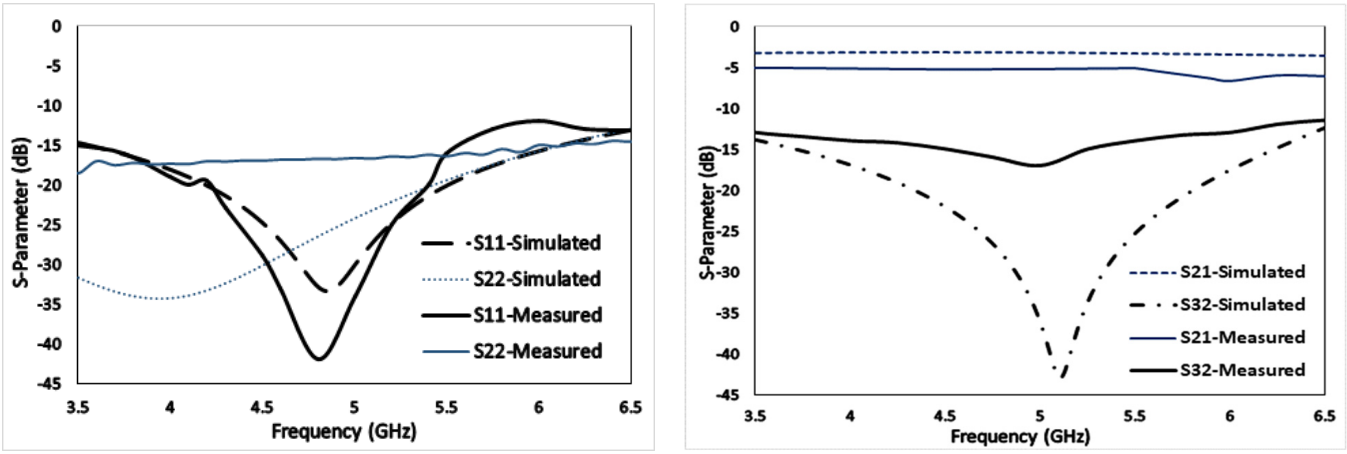

Figure 2. Shows the S−parameter response of the WPD (**a**) simulated and measured return loss (S_{11}) at port-1 and (S_{22}) at port-2, and (**b**) simulated and measured insertion loss (S_{21}) between port-1 and port-2, and isolation loss (S_{32}) between port-2 and port-3, respectively.

The return loss S_{11} (dB) and S_{22} (dB) at port-1 and port-2, as shown in Figure 2a, also refers to the fact that the designed delta-stub-based 1 × 2 WPD has a wide bandwidth of

3 GHz. Figure 2b shows the simulated and measured insertion loss S_{21} (dB) between port-1 and port-2, and isolation loss S_{32} (dB) between port-2 and port-3, respectively. It can be observed from the WPD measured response that there is an isolation of 14 dB between the two output ports and an insertion loss of -4 ± 1 dB between port-1 and port-2.

3. Single-Element Minkowski–Sierpinski Fractal Antenna and Four-Element Antenna Array Design and Characterization Results

3.1. Single-Element Fractal Antenna Design

In this section, a single-element Minkowski–Sierpinski fractal antenna design is discussed. In order to realize the single-element fractal antenna, the square-shaped MPA, as shown in Figure 3a, is initially designed by using the transmission-line model [8]. CST Microwave Studio is used to simulate and study the behavior of the antenna. Two different substrates materials are employed for this purpose, i.e., a high-end Rogers TMM4 substrate (h = 1.524 mm, ε_r = 4.5, $tan\ \delta$ = 0.002) and low-end FR4 epoxy glass substrate (h = 1.6 mm, ε_r = 4.3, $tan\ \delta$ = 0.02). The step-by-step procedure of fractal antenna design is shown in Figure 3a–c, and a detailed explanation is also provided in [22]. In step one of the design, a square MPA of length and width equal to 38.5 mm is realized. In step two of the design, the Minkowski carpet structure is applied to the square MPA as shown in Figure 3b based on the calculations from Equations (1)–(4) by choosing the values of a_1 and a_2 to be 0.64, and 0.064, respectively.

$$N_n = 8^n \tag{1}$$

$$L_n = \left(\frac{1}{3}\right)^n \tag{2}$$

$$w_1{}^{(n+1)} = a_1 \times L_n \tag{3}$$

$$w_2{}^{(n+1)} = a_2 \times L_n \tag{4}$$

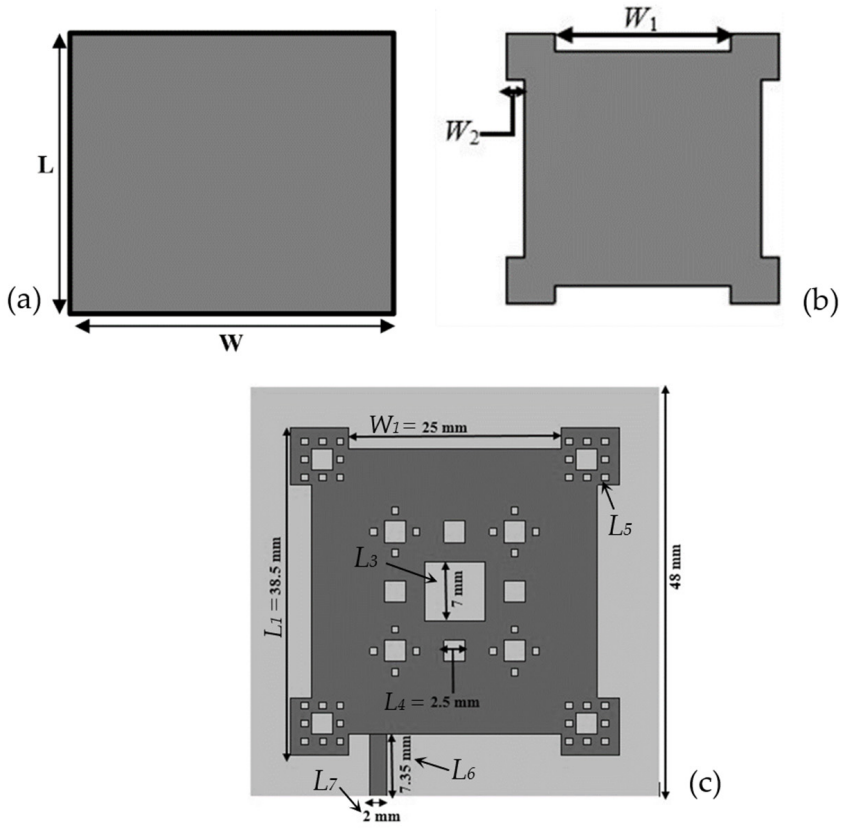

Figure 3. Shows (**a**) basic MPA with length "*L*" and width "*W*", (**b**) Minkowski structure introduced in basic MPA, and (**c**) combined Minkowski–Sierpinski carpet antenna design with respective dimensions.

In step three, the Sierpinski carpet structure is applied up to the third iteration to the remaining portion of step two, as shown in Figure 3c.

where L represents the length of the resonating patch, w_1 and w_2 are the dimensions of the rectangular slots removed from the sides of the square patch in the first iteration of this structure, and a_1 and a_2 refer to the indentation ratios, respectively. Table 1 shows the detailed dimensions of the single-element Minkowski–Sierpinski fractal antenna.

Table 1. Detailed dimensions of single-element combined Minkowski–Sierpinski carpet fractal antenna structure.

Antenna Dimensions	Value (Unit: mm)
L_1	38.5
W_1	25
L_3	7
L_4	2.5
L_5	0.8
L_6	7.35
L_7	2

The simulated S_{11} (dB) results of the proposed single-element Minkowski–Sierpinski fractal antenna design using two different substrates are summarized in Figure 4. It can be seen from the S_{11} (dB) result that the proposed antenna is resonating at dual frequency bands, i.e., around 4.1 and 5.97 GHz, respectively. After the S-parameter characterization of the single-element fractal antenna, the 2D radiation pattern results are also studied for a better understanding of antenna performance. Figure 5a–d shows the simulated E-plane and H-plane 2D radiation patterns of the FR4 and TMM4 substrate single-element fractal antennas. It can be seen from the radiation pattern results that the FR4-based single-element antenna exhibits a higher gain at 5.97 GHz, whereas the antenna designed using the TMM4 substrate only shows improvement at low frequency. It is important to observe from the results that the proposed antenna simulated using the FR4 substrate shows a gain of 0.8/7 dB at 4.17/5.97 GHz, respectively. Similarly, using the TMM4 substrate, the antenna exhibits a gain of 2.2/5.5 dB at 4.17/5.97 GHz, respectively. The proposed antenna's primary application is to work at Wi-Fi6 [5,6] and sub-6 GHz 5G systems, which means we need enhanced gain at a higher frequency. Due to this reason, the FR4-based single-element Minkowski–Sierpinski fractal antenna design is selected for fabrication and further characterization using a 2 × 2 antenna array design. Figure 6a shows the final structure of the single-element Minkowski–Sierpinski fractal antenna designed using the FR4 substrate.

Figure 6b shows the single-element antenna measurements setup using a Keysight Technologies FieldFox N9916B vector network analyzer (VNA). It can be seen from Figure 6b that the antenna under test (AUT) was resonating at two different frequencies of 4.17 and 5.97 GHz, respectively.

3.2. Four-Element (2 × 2 Configuration) Minkowski–Sierpinski Fractal Antenna Array (MSFAA) Design and Characterization

The key demand for the IEEE 802.11ax WLANs (Wi-Fi 6E), currently deployed 5G wireless systems, and next-generation wireless technologies is to have high-gain, directional, and narrow beam-width antenna arrays. Therefore, a four-element (2 × 2 configuration) MSFAA has been designed, fabricated, and realized using four single-element antennas, as shown in Figure 7a,b. Therefore, initially, the four-element MSFAA is simulated using CST Microwave Studio, and the results are summarized in Figure 8.

Then, the antenna array is realized, and the prototype is illustrated in Figure 7a,b, which shows the hybrid implementation of the MSFAA. Figure 7a shows the front, and

Figure 7b shows the back view of the four-element MSFAA prototype with detailed dimensions and connection configurations, respectively. An aluminum sheet of 240 × 240 mm is used to hold the antennas with the help of screws, as shown in Figure 7b. The aluminum sheet with a thickness of 2 mm also acts as an extended ground plane for the four-element MSFAA, as shown in Figure 7a,b. The 1 × 2 WPDs presented previously are used as a part of the antenna array feeding network to feed equal power to the four elements of the MSFAA. It can be seen in Figure 7a,b that we used small RF co-axial cables to make the connection between the main MSFAA feed point and the three 1 × 2 WPDs. In order to reduce the grating and radiation side lobes, the spacing between the center of one antenna and another is a key factor while designing the antenna array. Therefore, the spacing between the antenna elements (center-to-center spacing) is kept at 0.7 λ_0, i.e., 75 mm for the MSFAA. It can be seen from Figure 7b that co-axial cables, SMA connectors, and adapters are used to connect the three 1 × 2 WPDs to the individual antenna element feeds.

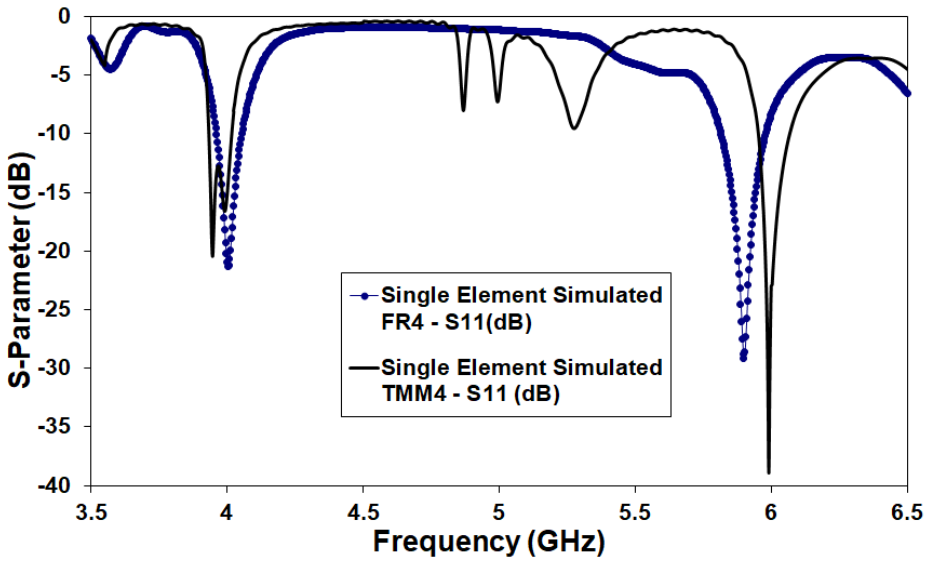

Figure 4. Simulated S_{11} (dB) response of the single−element Minkowski−Sierpinski fractal antenna using low−end FR4 and high−end Rogers TMM4 substrates.

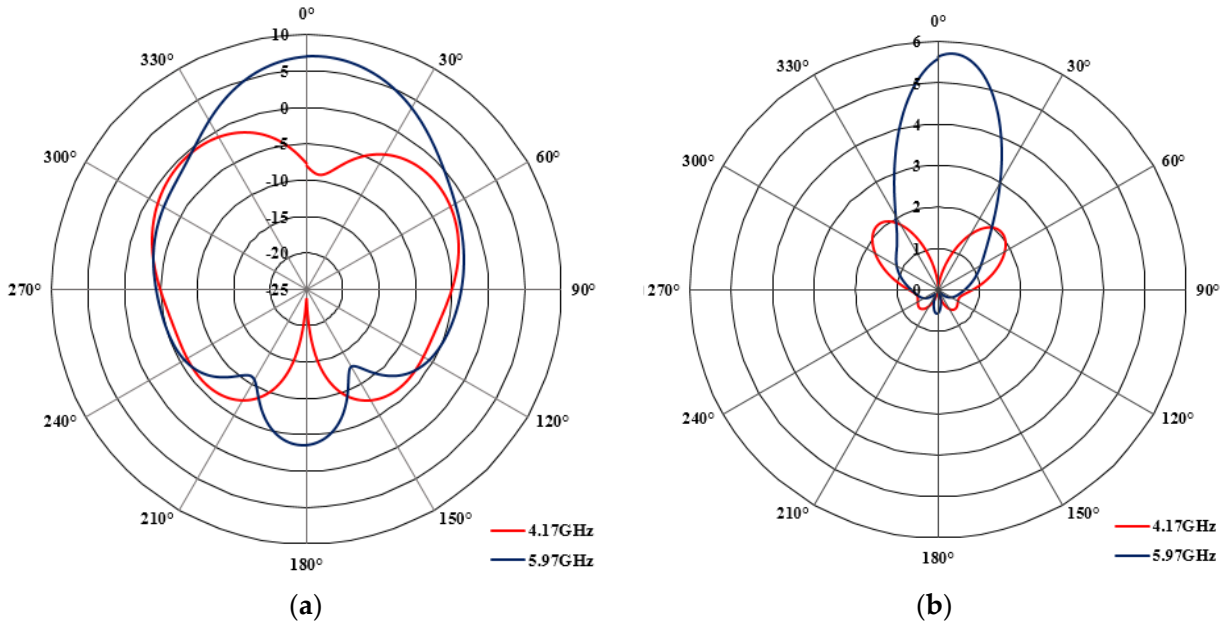

Figure 5. *Cont.*

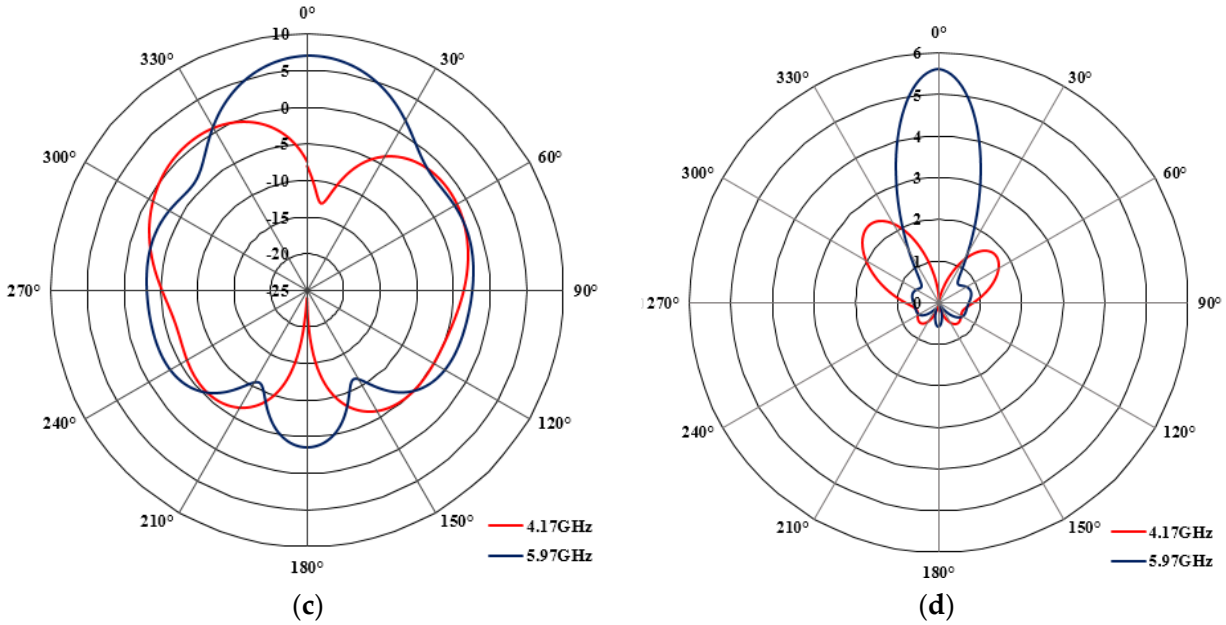

Figure 5. Simulated E−plane 2D radiation pattern of single-element antenna using (**a**) FR4 and (**b**) TMM4 substrates at 4.17 and 5.97 GHz, respectively, and simulated H−plane 2D radiation pattern of single−element antenna using (**c**) FR4 and (**d**) TMM4 substrates at 4.17 and 5.97 GHz, respectively.

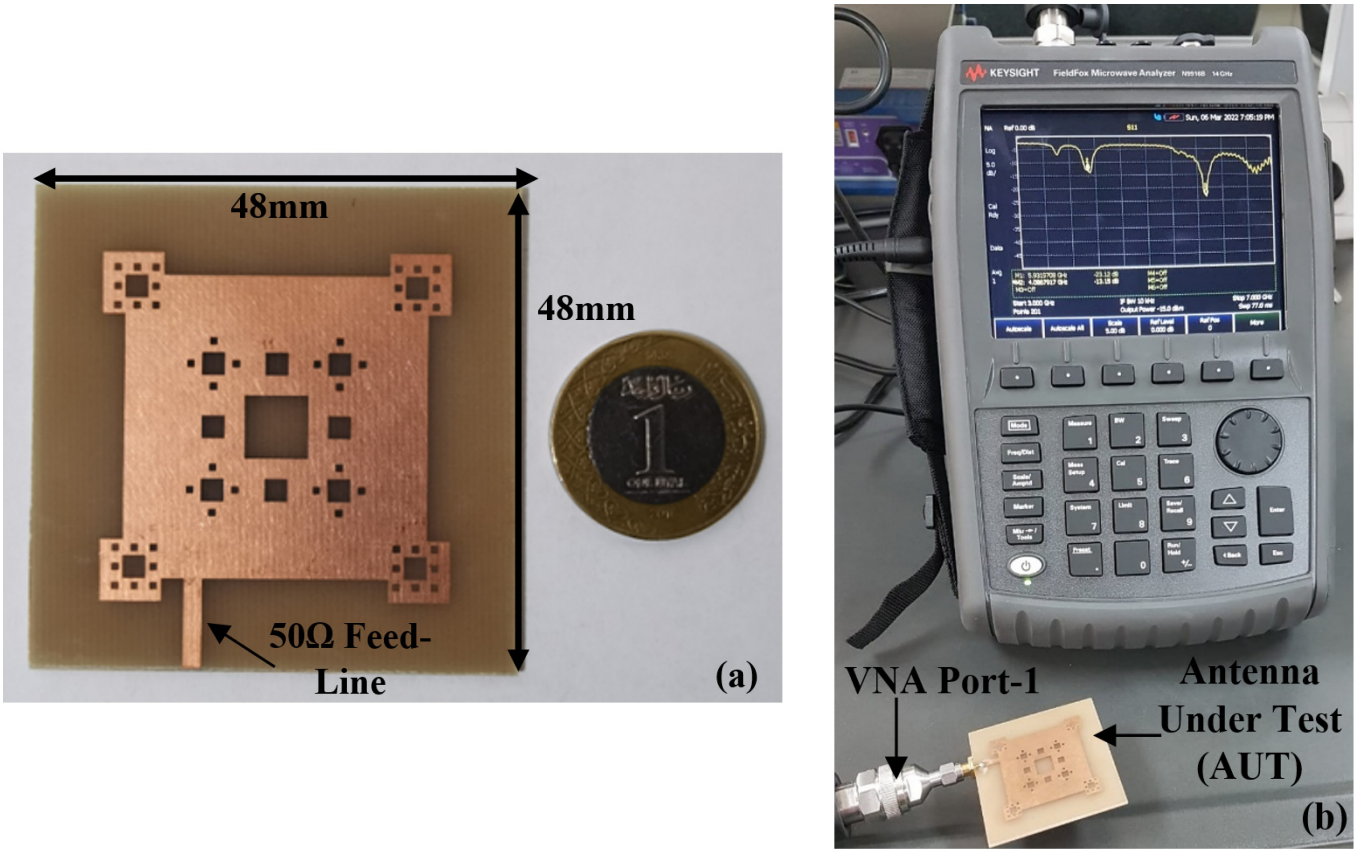

Figure 6. Shows (**a**) fabricated prototype of single-element combined Minkowski–Sierpinski fractal antenna using FR4 substrate, and (**b**) S-parameter measurement setup showing the AUT connected to Keysight VNA for S_{11} (dB) measurement.

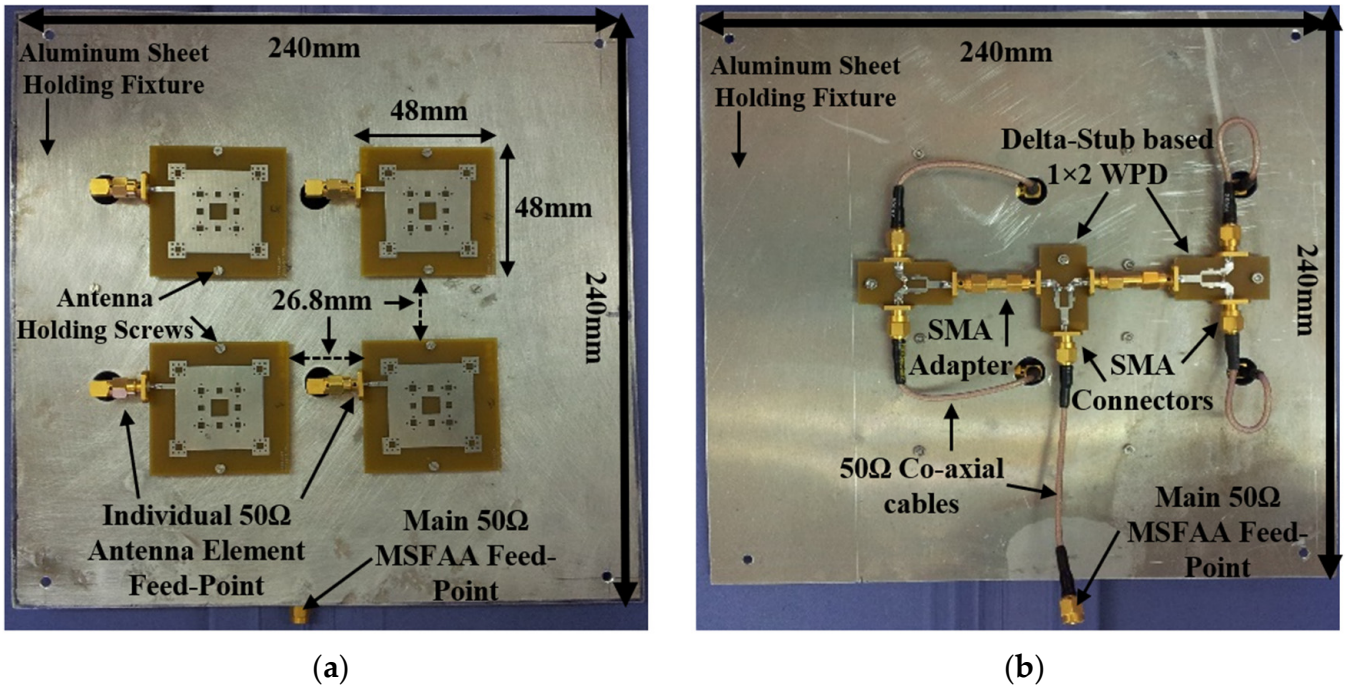

Figure 7. Shows (**a**) front view of a fabricated prototype of four-element MSFAA with dimensions, and (**b**) back view highlighting the four-element MSFAA feed network using WPDs and co-axial cables.

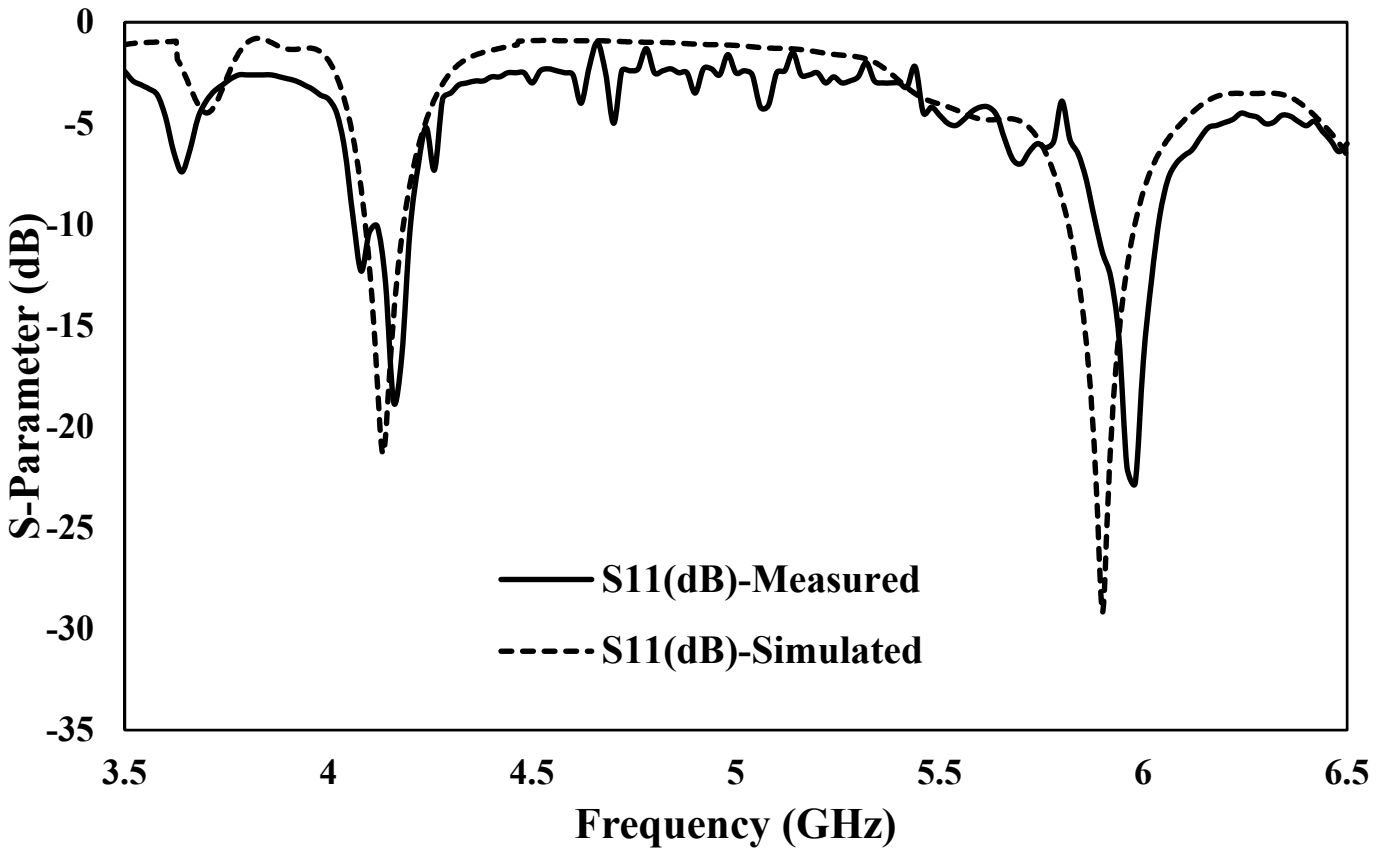

Figure 8. Shows the simulated and measured return loss S_{11} (dB) of the four−element MSFAA.

After the successful fabrication of the four-element MSFAA prototype, the S-parameter measurements are initially performed. Figure 8 compares the simulated and measured return loss S_{11} (dB) of the four-element MSFAA. It can be seen from the results in Figure 8

that the four-element MSFAA is operating at the two desired frequency bands for IEEE 802.11ax WLANs (Wi-Fi 6E), and 5G wireless systems operation with very good bandwidth and an S_{11} (dB) response of more than −17 and −25dB is achieved at 4.17 and 5.97 GHz, respectively.

It can also be observed from Figure 8 that the 2 × 2 configuration MSFAA has the simulated bandwidth of 96 and 165 MHz, around 4.17 and 5.97 GHz, respectively. Similarly, the measured S_{11} (dB) response of the fractal antenna array exhibits a bandwidth of 85 and 182 MHz, around 4.17 and 5.97 GHz, respectively. After the return loss measurements, the 2D and 3D radiation patterns and surface current distribution measurements of the four-element MSFAA are performed to further investigate and understand the behavior of the proposed antenna array for IEEE 802.11ax WLANs (Wi-Fi 6E) and the upcoming 5G wireless systems. The radiation pattern measurements are performed in a NI-800F anechoic chamber using a Keysight N5230A VNA. Figure 9a–d shows the simulated and measured E- and H-plane 2D radiation patterns of the four-element MSFAA, respectively. In Figure 9a, the simulated and measured E-plane 2D radiation patterns at 4.17 GHz are shown, where the MSFAA exhibits a 3 dB beamwidth of 34.8 and 31 °C, and a gain of 4.9 and ~4.2 dB, respectively. In Figure 9b, the simulated and measured H-plane 2D radiation patterns at 4.17 GHz are shown, where the MSFAA exhibits a 3 dB beamwidth of 36.8 and 32 °C, and a gain of 5.5 and ~5 dB, respectively. Similarly, in Figure 9c, the simulated and measured E-plane 2D radiation patterns are shown at 5.97 GHz, where the MSFAA exhibits a 3 dB beamwidth of 17.5 and 26.2 °C, and a gain of ~10.5 dB and ~9.6 dB, respectively. In Figure 9d, the simulated and measured H-plane 2D radiation patterns at 5.97 GHz are shown, where the MSFAA exhibits a 3 dB beamwidth of 17.1 and 28 °C, and a gain of 10 and ~9.8 dB, respectively. It can be observed from Figure 9a–d that the four-element MSFAA is radiating in the boresight at both resonating frequencies.

Moreover, the MSFAA exhibits more directional behavior at the high frequency than the low frequency of resonance, and the null is reduced at zero degrees in the E- and H-plane at 4.17 GHz. It is also important to observe here that the radiation pattern is directed away from the antenna with much-reduced back radiation by virtue of the presence of the extended ground plane in the form of an aluminum sheet. This is more prominent at the 5.97 GHz frequency, thus making the proposed fractal antenna array design more suitable to work in the high-efficiency IEEE 802.11ax WLANs (Wi-Fi 6E) and upcoming 5G wireless systems.

After measuring the 2D radiation pattern of the four-element MSFAA, the 3D radiation patterns are also studied at both the oscillating frequencies of 4.17 and 5.97 GHz to further understand the fractal antenna array behavior, and the results are summarized in Figure 10a,b, respectively. It can be observed from the 3D radiation patterns in Figure 10a,b that at 4.17 GHz resonance frequency, the antenna gain is 6.8 dB, but at the 5.97 GHz frequency, the antenna gain increases to 11.85 dB. The results show the directionality of the radiating electromagnetic waves from the proposed design, which is an important requirement for both high-efficiency IEEE 802.11ax WLANs and the upcoming 5G wireless systems for smart antenna beam-forming and beam-steering technologies [1–3,6,12].

It can be observed from the results in Figure 11a,b that when the antenna array is excited, the surface current distribution is high near to and around the resonating fractal patch antennas and low around the rest of the aluminum sheet, especially at the edges, which is acting as an extended ground plane.

The co- and cross-polarization analysis of the four-element MSFAA is then performed. The results of the co- and cross-polarization of the four-element MSFAA for E- and H-plane at 4.17 and 5.97 GHz, respectively, are illustrated in Figure 12a,b. The proposed four-element MSFAA shows E- and H-plane cross-polarization isolation of −13 and −17 dB at 4.17 GHz, respectively, as depicted in Figure 12a. In Figure 12b, it can be observed that E- and H-plane cross-polarization isolation of below −10 dB at 5.97 GHz is achieved.

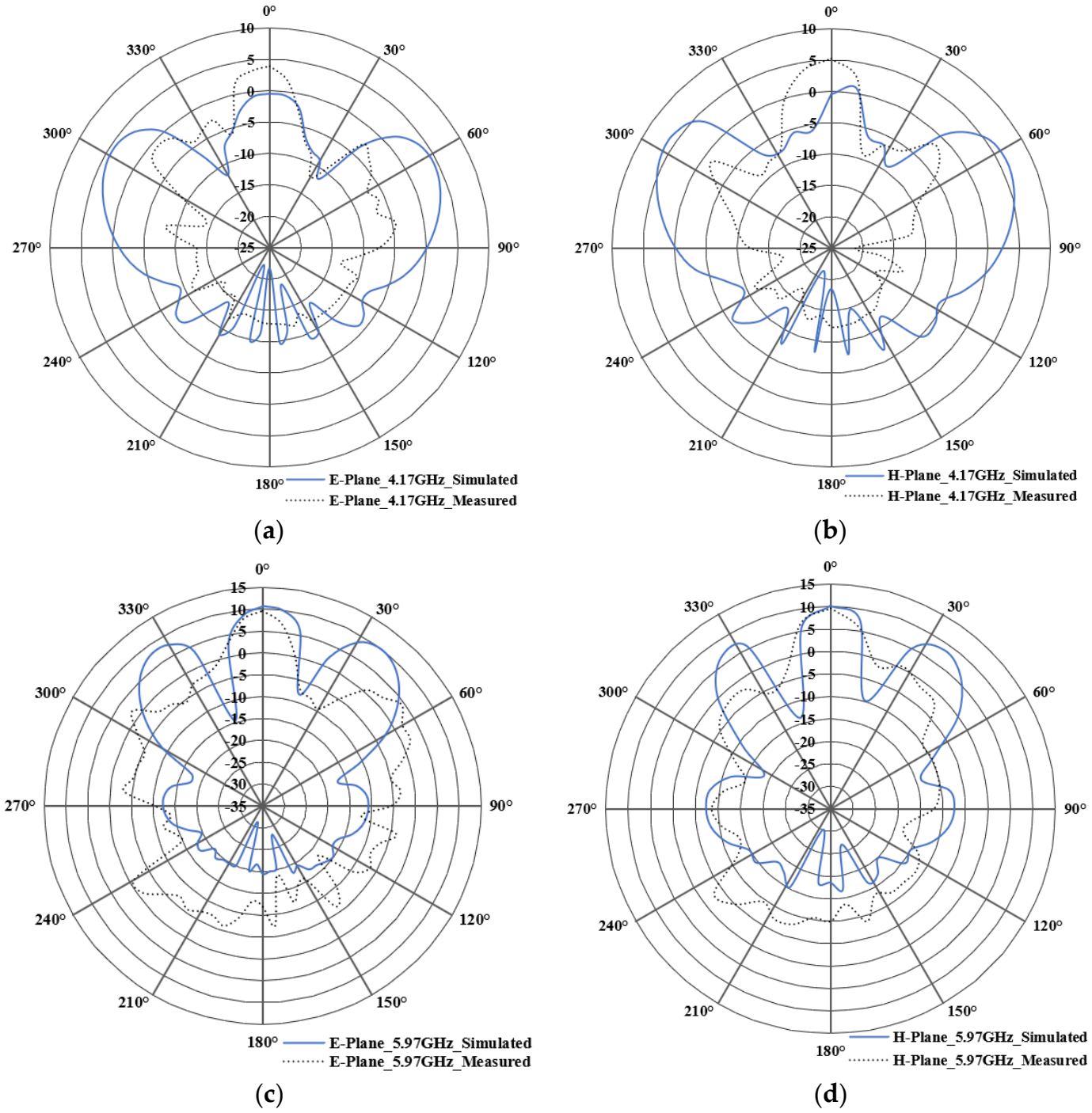

Figure 9. Shows simulated and measured (**a**) E−plane 2D radiation pattern at 4.17 GHz, (**b**) H−plane 2D radiation pattern at 4.17 GHz, (**c**) E-plane 2D radiation pattern at 5.97 GHz, and (**d**) H−plane 2D radiation pattern at 5.97 GHz, respectively, for the four−element MSFAA.

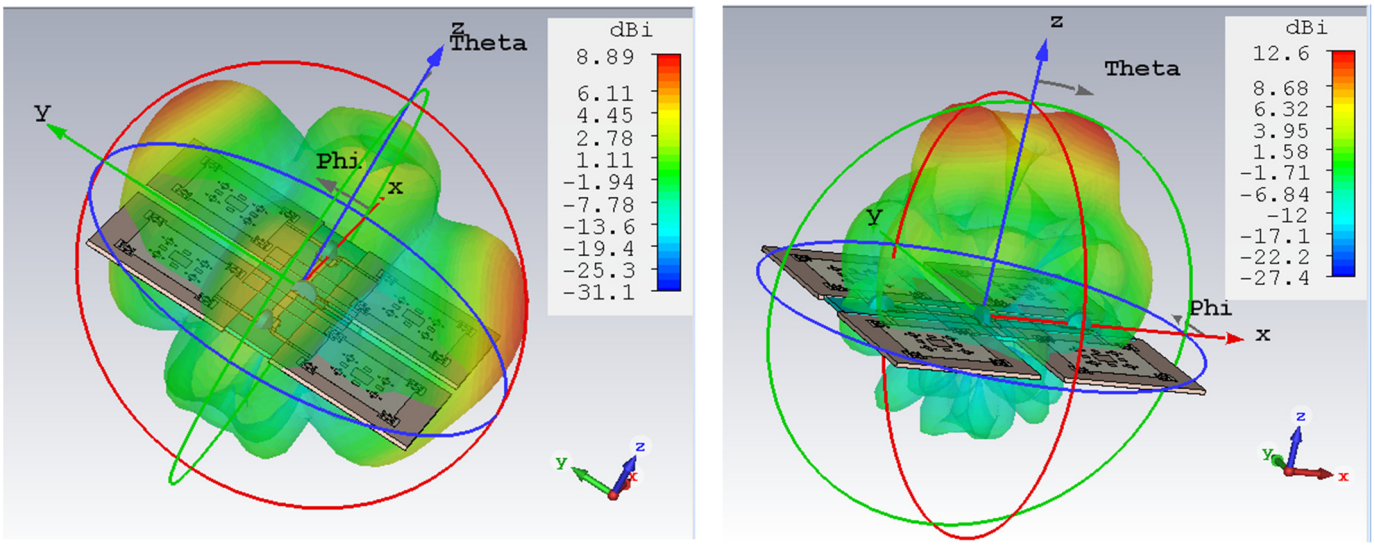

(**a**) (**b**)

Figure 10. Shows 3D radiation patterns of four-element MSFAA at (**a**) 4.17 GHz (gain 8.89 dB) and (**b**) 5.97 GHz (gain 12.6 dB), respectively.

After measuring the 3D radiation patterns, the surface current distribution of the four-element MSFAA is studied to further understand the behavior of the fractal antenna array when excited with electromagnetic waves. Figure 11a,b shows the fractal antenna array response at 4.17 and 5.97 GHz, respectively.

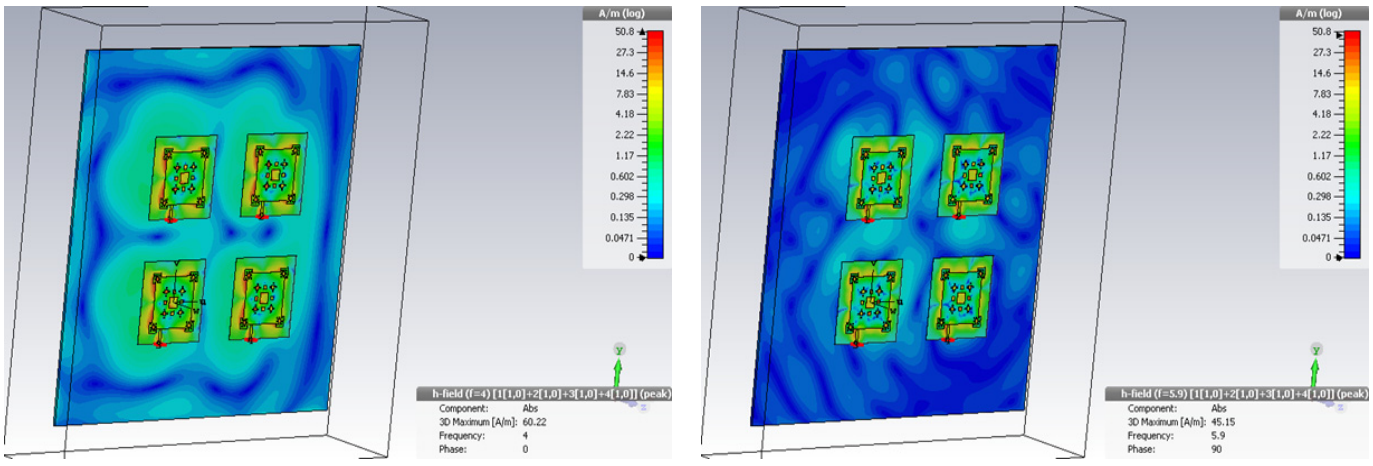

(**a**) (**b**)

Figure 11. Shows surface current distribution of 4-element MSFAA at (**a**) 4.17 GHz and (**b**) 5.97 GHz, respectively.

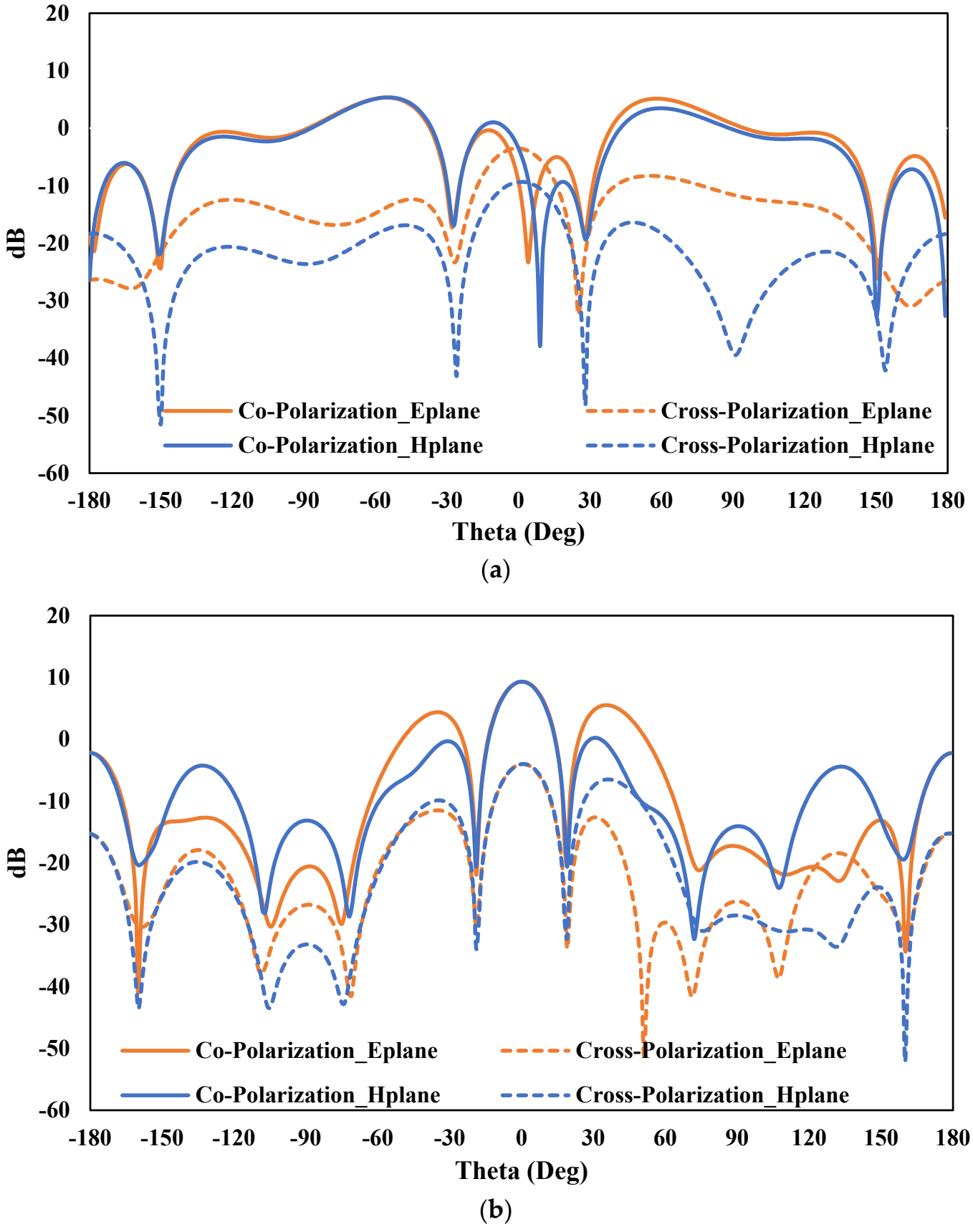

Figure 12. Shows the co− and cross−polarization analysis of the four−element MSFAA for E− and H−plane at (**a**) 4.17 GHz and (**b**) 5.97 GHz, respectively.

4. Comparison of Results and Discussion

It has been observed in the previous section from the 2D and 3D radiation pattern results that at 5.97 GHz, MSFAA gain and directionality are greater as compared to low frequency at 4.17 GHz, but the important factor is that the null is reduced at zero degrees in the E- and H-plane at 4.17 GHz. This leads to a better radiation pattern with fewer side lobes. Moreover, it is evident from the 2D and 3D radiation patterns that the four-element (2×2 configuration) MSFAA demonstrates reduced back radiation and improved directionality at both resonant frequencies. Therefore, the advantage of high gain and directional radiation patterns in the boresight makes the proposed fractal antenna array design more suitable to work in the currently deployed high-efficiency IEEE 802.11ax WLANs (Wi-Fi 6E) and the upcoming 5G systems. Additionally, the directional antenna array can be very useful in the intelligent transport system and Internet of Vehicles (IoV) [33,34] system, where vehicle-to-vehicle (V2V) and vehicle-to-infrastructure (V2I) communications heavily rely on directional beam-steering antenna array systems. Another potential area of application for the single-element antenna and antenna arrays is flying ad hoc networks (FANETs) [35], where unmanned aerial vehicles (UAVs) are employed for both commercial and military communications [36]. In FANETs, wireless communication links are required for UAV-to-UAV (U2U) and UAV-to-base station (U2B) communications [37]. Table 2 summarizes the comparison of the proposed four-element Minkowski–Sierpinski fractal antenna array simulated and measured results. The data in Table 2 show good agreement between the simulated and measured results of the four-element fractal antenna array.

Table 2. Comparison of simulation and measured results of four-element MSFAA.

Parameter	MSFAA Simulation Results		MSFAA Measurement Results	
	4.17 GHz	**5.97 GHz**	**4.17 GHz**	**5.97 GHz**
Return loss (dB)	21.2	29.1	17.1	25.8
Bandwidth (MHz) (for VSWR < 2)	96	165	85	182
Gain (dB)	4.9	10.5	4.19	9.6
E-plane Beamwidth (Deg)	34.8	17.5	31	26.2
H-plane Beamwidth (Deg)	36.8	17.1	32	28

Table 3 gives a detailed comparison of the existing work carried out on fractal antenna arrays with respect to proposed antenna array design techniques in terms of multiband operation, gain, bandwidth, radiation pattern, and efficiency. From Table 3, it is very important to note that in most of the presented designs, the researchers are improving one antenna performance parameter only, such as gain or the bandwidth, although the work presented in this paper shows the overall improvement of all antenna performance parameters, as mentioned in Table 3.

Table 3. Performance comparison of proposed four-element MSFAA with existing research literature where other researchers have proposed antenna arrays using fractal structures.

Reference/Year	Multiband	Technique	Maximum Gain (dB)	Radiation Efficiency	Radiation Pattern in Boresight for All Frequency Bands	No. of Antenna Elements	Bandwidth (MHz)	Antenna Spacing
[23]/2019	Yes	Circular fractal array	5.94	-	No	4	~500	0.5λ
[24]/2018	Yes	Koch-fed obtrude/slot asymmetric ground plane	5	93%	No	4	~104	-
[25]/2019	No	Fibonacci series with the incorporation of Koch snowflake structure	15.18	72.12%	No	4	105	0.5λ
[26]/2018	Yes	Sierpinski carpet fractal antenna array	11	-	No	8	90	0.9λ
[27]/2014	Yes	Fractal tree antenna array	9.3	-	No	4	~40	-
[28]/2019	No	Complementary Sierpinski gasket fractal antenna array	9.98	68%	No	4	~400	-
[29]/2022	Yes	Rectangular and circular patch antenna array	5.71	97%	No	16	980	0.3λ
[30]/2019	Yes	Rectangular slotted patch antenna array	4.5	-	No	2	930	0.24λ
[31]/2021	Yes	Tri-band hexagonal fractal antenna array	4.2	-	No	2	300	-
[32]/2018	Yes	Sierpinski carpet fractal antenna array	2.82	-	No	2	~40	0.7λ
[38]/2018	No	Patch antenna arrays based on fractal metamaterial EBG structures	~5.5	~81%	No	4	1250	0.5λ
[39]/2022	Yes	Metasurface-inspired fractal antenna	7.7	~80%	Yes	-	244	-
[40]/2020	No	Koch-snowflake-based fractal antenna	11	71%	Yes	4	165	0.5λ
[This Work]/2022	Yes	Combined Minkowski–Sierpinski carpet antenna	9.61	96%	Yes	4	182	0.7λ

5. Conclusions

This paper has presented a dual-band and low-profile single-element Minkowski–Sierpinski fractal antenna and a high-gain, directional four-element (2 × 2 configuration) Minkowski–Sierpinski fractal antenna array resonating at 4.17 and 5.97 GHz. The single-element antenna was initially designed using two different substrates, i.e., a high-end Rogers TMM4 and a low-end FR4 substrate. In order to feed the fractal antenna array, a Wilkinson power divider based on delta-stub was also designed to achieve a wide band and equal power split from the input ports to all four elements of the fractal antenna array. It is important to observe here that most of the previous dual-band antenna arrays presented in Table 3 radiate in the boresight at only one frequency and the other frequency is null, but the proposed four-element fractal antenna array from this work has a radiation pattern in the boresight at both resonant frequencies with high gain and good bandwidth. Due to this unique feature of the radiation pattern, the proposed antenna array can act as an ideal candidate for currently deployed high-efficiency IEEE 802.11ax WLANs (Wi-Fi 6E), the upcoming 5G wireless systems, the IoV, and FANETs system, where V2V/V2I and U2U/U2B wireless communication links are heavily dependent on the directional beam-steering capabilities of the antenna arrays. The proposed antenna array shows very good agreement between the simulated and measured results. The results show that the proposed structure is a promising candidate for IEEE 802.11ax WLANs (Wi-Fi 6E) and future 5G wireless communication. In the future, this work can be extended by reducing the overall size of the array using the combination of all the components on the single ground plane and removing the coaxial cable and other non-essential components to check and study the overall behavior of the antenna array system.

Author Contributions: A.K.V. and B.A.K. coined the idea, led, supervised, and evaluated the entire project, edited the write-ups, designed and simulated the proposed antennas. A.K.V., B.A.K. and M.K.A.R. performed the experimental measurements. A.K.V. completed the initial draft of the paper; A.K.V., B.A.K., M.K.A.R., M.U., M.J. and Q.A. then analyzed, evaluated, and edited the paper. All authors have read and agreed to the published version of the manuscript.

Funding: This research was funded by the "Deanship of Scientific Research, Islamic University of Madinah, Madinah, Saudi Arabia, Grant Number 171".

Institutional Review Board Statement: Not Applicable

Informed Consent Statement: Not Applicable

Data Availability Statement: Not Applicable

Acknowledgments: The authors would like to acknowledge the funding from the Deanship of Scientific Research, Islamic University of Madinah, Madinah, Saudi Arabia, under the Research Grant No. 171.

Conflicts of Interest: The authors declare no conflict of interest.

References

1. Akyildiz, I.F.; Han, C.; Hu, Z.; Nie, S.; Jornet, J.M. Terahertz Band Communication: An Old Problem Revisited and Research Directions for the Next Decade. *IEEE Trans. Commun.* **2022**, *70*, 4250–4285. [CrossRef]
2. Shafique, K.; Khawaja, B.A.; Sabir, F.; Qazi, S.; Mustaqim, M. Internet of Things (IoT) for Next-Generation Smart Systems: A Review of Current Challenges, Future Trends and Prospects for Emerging 5G-IoT Scenarios. *IEEE Access* **2020**, *8*, 23022–23040. [CrossRef]
3. Rappaport, T.S.; Xing, Y.; Kanhere, O.; Ju, S.; Madanayake, A.; Mandal, S.; Alkhateeb, A.; Trichopoulos, G.C. Wireless Communications and Applications Above 100 GHz: Opportunities and Challenges for 6G and Beyond. *IEEE Access* **2019**, *7*, 78729–78757. [CrossRef]
4. Statista Research Department. Internet of Things (IoT) Connected Devices Installed Base Worldwide from 2015 to 2025. 27 November 2016. Available online: www.statista.com/statistics/471264/iot-number-of-connected-devices-worldwide/ (accessed on 15 September 2022).

5. Nasir, S.A.; Mustaqim, M.; Khawaja, B.A. Antenna Array for 5th Generation 802.11ac Wi-Fi Applications. In Proceedings of the 11th International Conference on High-capacity Optical Networks & Emerging Technologies (HONET), UNC Charlotte, NC, USA, 15–17 December 2014.
6. Khorov, E.; Kiryanov, A.; Lyakhov, A.; Bianchi, G. A Tutorial on IEEE 802.11ax High Efficiency WLANs. *IEEE Commun. Surv. Tutor.* **2019**, *21*, 197–216. [CrossRef]
7. Khawaja, B.A.; Cryan, M.J. Study of Millimeter Wave Phase Shift in 40 GHz Hybrid Mode Locked Lasers. *IEEE Microw. Wirel. Compon. Lett.* **2009**, *19*, 182–184. [CrossRef]
8. Balanis, C.A. *Antenna Theory, Analysis and Design*, 3rd ed.; John Wiley & Sons, Inc.: Hoboken, NJ, USA, 2005.
9. Wong, H.; Luk, K.-M.; Chan, C.H.; Xue, Q.; So, K.K.; Lai, H.W. Small Antennas in Wireless Communications. *Proc. IEEE* **2012**, *100*, 2109–2121. [CrossRef]
10. Tan, M.C.; Li, M.; Abbasi, Q.H.; Imran, M. A Wideband Beam forming Antenna Array for 802.11ac and 4.9 GHz. In Proceedings of the Antennas and Propagation (EuCAP) 2019 13th European Conference, Krakow, Poland, 31 March–5 April 2019; pp. 1–5.
11. Kim, J.H.; Han, J.H.; Park, J.S.; Kim, J.G. Design of phased array antenna for 5G mm-wave beamforming system. In Proceedings of the 2016 IEEE 5th Asia-Pacific Conference on Antennas and Propagation (APCAP), Kaohsiung, Taiwan, 26–29 July 2016; pp. 201–202.
12. Karimbu Vallappil, A.; Khawaja, B.A.; Rahim, M.K.A.; Iqbal, M.N.; Chattha, H.T. Metamaterial-Inspired Electrically Compact Triangular Antennas Loaded with CSRR and 3 × 3 Cross-Slots for 5G Indoor Distributed Antenna Systems. *Micromachines* **2022**, *13*, 198. [CrossRef]
13. Sharawi, M.S. A 5-GHz 4/8-element MIMO antenna system for IEEE 802.11ac devices. *Microw. Opt. Technol. Lett.* **2013**, *55*, 1589–1594. [CrossRef]
14. Vallappil, A.K.; Rahim, M.K.A.; Khawaja, B.A.; Iqbal, M.N.; Murad, N.A.; Gajibo, M.M.; Nur, L.O.; Nugroho, B.S. Complementary split-ring resonator and strip-gap based metamaterial fractal antenna with miniature size and enhanced bandwidth for 5G applications. *J. Electromagn. Waves Appl.* **2022**, *36*, 787–803. [CrossRef]
15. Abed, A.T.; Jawad, A.M. Compact Size MIMO Amer Fractal Slot Antenna for 3G, LTE (4G), WLAN, WiMAX, ISM and 5G Communications. *IEEE Access* **2019**, *7*, 125542–125551. [CrossRef]
16. Yu, Z.; Yu, J.; Ran, X.; Zhu, C. A novel Koch and Sierpinski combined fractal antenna for 2G/3G/4G/5G/WLAN/navigation applications. *Microw. Opt. Technol. Lett.* **2017**, *59*, 2147–2155. [CrossRef]
17. Jilani, S.F.; Aziz, A.K.; Abbasi, Q.H.; Alomainy, A. Ka-band Flexible Koch Fractal Antenna with Defected Ground Structure for 5G Wearable and Conformal Applications. In Proceedings of the 2018 IEEE 29th Annual International Symposium on Personal, Indoor and Mobile Radio Communications (PIMRC), Bologna, Italy, 9–12 September 2018.
18. Mandelbrot, B.B. *The Fractal Geometry of Nature*; W. H. Freeman and Company: New York, NY, USA, 1982; ISBN 978-0716711865.
19. Fan, J.A.; Yeo, W.-H.; Su, Y.; Hattori, Y.; Lee, W.; Jung, S.-Y.; Zhang, Y.; Liu, Z.; Cheng, H.; Falgout, L.; et al. Fractal design concepts for stretchable electronics. *Nat. Commun.* **2014**, *5*, 3266. [CrossRef]
20. Oraizi, H.; Hedayati, S. Miniaturized UWB Monopole Microstrip Antenna Design by the Combination of Giusepe Peano and Sierpinski Carpet Fractals. *IEEE Antennas Wirel. Propag. Lett.* **2011**, *10*, 67–70. [CrossRef]
21. Manimegalai, B.; Raju, S.; Abhaikumar, V. A Multifractal Cantor Antenna for Multiband Wireless Applications. *IEEE Antennas Wirel. Propag. Lett.* **2009**, *8*, 359–362. [CrossRef]
22. Vallappil, A.K.; Khawaja, B.A.; Khan, I.; Mustaqim, M. Dual-Band Minkowski-Sierpinski Fractal Antenna for Next Generation Satellite Communications and Wireless Body Area Networks. *Microw. Opt. Technol. Lett.* **2018**, *60*, 171–178. [CrossRef]
23. Chauhan, R.; Gupta, S. A Circular Fractal Antenna Array. In Proceedings of the 2019 National Conference on Communications (NCC), Bangalore, India, 20–23 February 2019; pp. 1–6.
24. Mohanty, A.; Sahu, S. Koch-fed-Obtrude/Slot AGP Fractal Antennas for Wideband Applications. In Proceedings of the 2018 IEEE Indian Conference on Antennas and Propagation (InCAP), Hyderabad, India, 16–19 December 2018; pp. 1–3.
25. Patanvariya, D.G.; Chatterjee, A.; Kola, K.; Naik, S. Design of a linear array of fractal antennas with high directivity and low cross-polarization for dedicated short range communication application. *Int. J. RF Microw. Comput.-Aided Eng.* **2019**, *1*, e22038. [CrossRef]
26. Kumar, A.; Partap, A. On the Design of 2×2 Element Fractal Antenna Array using Dragonfly Optimization. *Int. J. Comput. Appl.* **2018**, *179*, 27–34. [CrossRef]
27. Anitha, D.V.R. A Novel Design of Rectangular Antenna Array Using Fractal Tree Structure. *Proceeding of URSI procGA14, ursi_paper2340*. 2014. Available online: https://www.ursi.org/proceedings/procGA14/papers/ursi_paper2340.pdf (accessed on 24 July 2022).
28. Kaur, A.; Gupta, S. A complementary Sierpinski gasket fractal antenna array for wireless MIMO portable devices. *Microw. Opt. Technol. Lett.* **2019**, *61*, 436–442. [CrossRef]
29. Paul, L.C.; Ali, M.H.; Rani, T.; Saha, H.K.; Jim, M.T. A sixteen-element dual band compact array antenna for ISM/Bluetooth/Zigbee/WiMAX/WiFi-2.4/5/6 GHz applications. *Heliyon* **2022**, *8*, e11675. [CrossRef]
30. Tang, C.; Zheng, H.; Wang, M.; An, X.; Wang, X.; Li, E. A Dual-Band Antenna Array with High Gain and Miniaturized Structure. In Proceedings of the 2019 IEEE 2nd International Conference on Electronic Information and Communication Technology (ICEICT), Harbin, China, 20–22 January 2019; pp. 735–738.

31. Palanisamy; Satheeshkumar; Thangaraju, B.; Khalaf, O.I.; Alotaibi, Y.; Alghamdi, S.; Alassery, F. A novel approach of design and analysis of a hexagonal fractal antenna array (HFAA) for next-generation wireless communication. *Energies* **2021**, *14*, 6204. [CrossRef]
32. Prabhakar, D.; Rao, P.M.; Satyanarayana, M. Sierpinski Carpet Fractal Antenna Array Using Quarter-Wave Feed Network for Wireless Applications. In *Proceedings of 2nd International Conference on Micro-Electronics, Electromagnetics and Telecommunications*; Springer: Singapore, 2018; pp. 445–453. [CrossRef]
33. Kombate, D. Wanglina The Internet of Vehicles Based on 5G Communications. In Proceedings of the 2016 IEEE International Conference on Internet of Things (iThings) and IEEE Green Computing and Communications (GreenCom) and IEEE Cyber, Physical and Social Computing (CPSCom) and IEEE Smart Data (SmartData), Chengdu, China, 15–18 December 2016.
34. Qazi, S.; Sabir, F.; Khawaja, B.A.; Atif, S.M.; Mustaqim, M. Why is Internet of Autonomous Vehicles not as Plug and Play as We Think? Lessons to Be Learnt from Present Internet and Future Directions. *IEEE Access* **2020**, *8*, 133015–133033. [CrossRef]
35. Bekmezci, I.; Sahingoz, O.K.; Temel, Ş. Flying Ad-Hoc Networks (FANETs): A survey. *AdHoc Netw.* **2013**, *11*, 1254–1270. [CrossRef]
36. Walker, S.; Rice, D.; Kahn, M.; Clark, J. Why the World's Militaries Are Embracing 5G: To Fight on Tomorrow's More Complicated Battlefields, Militaries Must Adapt Commercial Technologies. IEEE Spectrum. 11 June 2022. Available online: https://spectrum.ieee.org/lockheed-martin-5g (accessed on 4 September 2022).
37. Mustaqim, M.; Khawaja, B.A.; Razzaqi, A.A.; Zaidi, S.S.H.; Jawed, S.A.; Qazi, S.H. Wideband and High Gain Antenna Arrays for UAV-to-UAV and UAV-to-Ground Communication in Flying Ad-Hoc Networks (FANETs). *Microw. Opt. Technol. Lett.* **2018**, *60*, 1164–1170. [CrossRef]
38. Alibakhshikenari, M.; Virdee, B.S.; See, C.H.; Abd-Alhameed, R.; Ali, A.H.; Falcone, F.; Limiti, E. Study on isolation improvement between closely-packed patch antenna arrays based on fractal metamaterial electromagnetic bandgap structures. *IET Microw. Antennas Propag.* **2018**, *12*, 2241–2247. [CrossRef]
39. Mohanty; Asutosh; Behera, B.R.; Esselle, K.P.; Alsharif, M.H.; Jahid, A.; Mohsan, S.A.H. Investigation of a Dual-Layer Metasurface-Inspired Fractal Antenna with Dual-Polarized/-Modes for 4G/5G Applications. *Electronics* **2022**, *11*, 2371. [CrossRef]
40. Patanvariya, D.G.; Chatterjee, A.; Kola, K.S. High-Gain and Circularly Polarized Fractal Antenna Array for Dedicated Short Range Communication Systems. *Prog. Electromagn. Res. C* **2020**, *101*, 133–146. [CrossRef]